frontiers | Frontiers in Energy Research

TYPE Original Research
PUBLISHED 08 August 2022
DOI 10.3389/fenrg.2022.964841

OPEN ACCESS

EDITED BY
Liangming Pan,
Chongqing University, China

REVIEWED BY
Longxiang Zhu,
Chongqing University, China
Liangxing Li,
Xi'an Jiaotong University, China

*CORRESPONDENCE
Hui Cheng,
chengh78@mail.sysu.edu.cn
Songbai Cheng,
chengsb3@mail.sysu.edu.cn

SPECIALTY SECTION
This article was submitted to Nuclear Energy,
a section of the journal
Frontiers in Energy Research

RECEIVED 09 June 2022
ACCEPTED 12 July 2022
PUBLISHED 08 August 2022

CITATION
Mai Z, Zhao Z, Cheng H, Cheng S and Zhao J (2022), Numerical study on the release and migration behavior of fission gas in a molten LBE pool.
Front. Energy Res. 10:964841.
doi: 10.3389/fenrg.2022.964841

Numerical study on the release and migration behavior of fission gas in a molten LBE pool

Zijun Mai[1], Zichen Zhao[2], Hui Cheng[1]*, Songbai Cheng[1]* and Jiyun Zhao[3]

[1]Sino-French Institute of Nuclear Engineering and Technology, Sun Yat-Sen University, Zhuhai, Guangdong, China, [2]Reactor Engineering Center/Serious Accident Department, China Nuclear Power Technology Research Institute Co., Ltd., Shenzhen, Guangdong, China, [3]Department of Mechanical Engineering, City University of Hong Kong, Hong Kong, China

The lead-cooled fast reactor (LFR) is one of the most promising fast neutron reactors using molten lead or the lead–bismuth eutectic (LBE) alloy as a coolant. Under postulated severe accidents, the fuel rod of LFR may be damaged, which would cause the release of fission gas, and the migration of fission gas bubbles in the reactor molten pool will affect the release and absorption of radioactive substances in the reactor. In this paper, a three-dimensional numerical study on the release and migration behavior of fission gas in the molten LBE pool of LFR is carried out based on the volume of fluid method. The bubbles are continuously released by gas injection, and the research mainly focuses on the detachment time, the rising velocity, and the size of the bubble when it detaches at the orifice. The coalescence of bubbles is observed, and the acceleration effect of the bubble wake is confirmed. The distribution of the bubble terminal rising velocity with diameter has no simple or linear relationship. The effects of the gas injection velocity, the release depth, and the gas injection angle are studied. A lower gas injection velocity will delay the detachment and reduce the size of the bubble. The increase of release depth tends to release smaller bubbles. The bubbles released from a vertical surface will attach to the wall. The simulations and theoretical analysis are comparable and have similar tendencies. The distribution of the bubble terminal rising velocity with equivalent diameter may predict the migration behavior of bubbles in molten LBE.

KEYWORDS

lead-cooled fast reactor, lead–bismuth eutectic alloy, bubble migration, VOF method, nuclear safety

Introduction

Fast neutron reactors can greatly improve the utilization rate of uranium resources and reduce nuclear contamination through transmutation as well as improve the safety during operation (Kelly, 2014; Pioro, 2016). As one of the members of fast neutron reactors using a liquid metal as a coolant (Pioro, 2016), the lead-cooled fast reactor (LFR) utilizes lead or lead-based alloys such as the lead–bismuth Eutectic alloy (LBE) as the primary coolant, which has favorable characteristics in terms of thermal properties,

chemical inertness, and a harder neutron spectrum (Tuček et al., 2006; Fazio et al., 2015). However, LFRs have not reached the level of commercial operation and exist only for a few experimental use and military applications (Cinotti et al., 2009).

In a pool-type LFR, the fuel assemblies are deployed in the molten LBE pool, and the fuel pellet undergoes the fission reaction, producing neutrons, solid fission products, and gas fission products. In a postulated severe accident, the core fuel rods suffer damages, the fission gas contained will be released from the crack, and gas bubbles will be formed in the LBE pool, which will affect the natural circulation of the primary loop and then influence the safety of the operation. Fission gas is a component of the radioactive source item of the coolant of the primary circuit. When the fission gas bubbles are formed, their volumes and migration behavior will directly affect the distribution of radioactive substances in the molten pool, causing changes in the absorption and release among the core, the coolant of the primary circuit, and the gas environment, which will affect the safety analysis of LFR, such as the analysis of the radioactive source term. Hence, fully understanding of the release and migration behavior of fission gas in the molten LBE pool is crucial for the safety design of LFR.

As a common phenomenon in various scenarios, the migration behavior of bubbles in the liquid has been studied by numerous researchers with theoretical analyses, experiments, and simulations. Dating back to 1917, the Rayleigh equation (Rayleigh, 1917) can describe the instantaneous pressure of the external liquid and the radius with time of a large bubble. Based on this, viscosity and surface tension have been considered in the Rayleigh–Plesset equation (Plesset and Chapman, 1971). The viscous drag is an important factor affecting the migration of bubbles; many researches have carried out studies on the drag coefficient (Prosperetti, 1977; Bhaga and Weber, 1981; Kang and Leal, 1988a; Kang and Leal, 1988b; Tomiyama et al., 1998). A large number of experiments and theoretical analyses have shown that the rising velocity of bubbles in the liquid is related to the size of the bubbles, and many scholars have proposed methods to calculate the rising velocity of bubbles based on different assumptions. Davies and Taylor (Davies and Taylor, 1950) studied the rising velocity of large bubbles and proposed the formula for the calculation. Based on this, Joseph's formula has considered viscosity and surface tension (Joseph, 2003). The analogy of the wave theory has been applied for the prediction of the terminal rising velocity of bubbles in surface tension- and inertia-dominated regions (Mendelson, 1967). In Wallis's drift model, the formulas of the terminal rising velocity of bubbles in still liquids under flow conditions distinguished by the Re number and Ga number are given (Wallis, 1974). Grace's graphical empirical correlation (Clift et al., 1987) interprets the shape of bubbles by three dimensionless numbers, namely, the Reynolds number (Re), the Morton number (Mo), and the Eötvös number (Eo), and it can be used to predict the terminal rising velocities of bubbles. Tomiyama et al. (2002) analyzed the relationship between the terminal rising velocity of the bubble and the aspect ratio that characterizes the deformation of the bubble through experiments and theoretical analysis and proposed a model of the relationship between the terminal rising velocity and the aspect ratio of the bubble.

Although theoretical and experimental studies have achieved certain results, most of them are based on spherical bubbles. For other complex flow conditions such as a high Reynolds number, large bubble deformation, and interaction between multiple bubbles, numerical simulation study shows its advantages. Zhang et al. (2012) used the volume of fluid (VOF) method to study the dynamic characteristics of the formation, growth, release, and rise of a single bubble in three dimensions, and the effects of fluid properties, fluid velocities, orifice number, and nozzle size on bubble behavior are investigated. Based on the finite element lattice Boltzmann method of mass conservation (FE-LBE), a two-dimensional (2D) numerical simulation study of bubbles rising in a viscous liquid at a high Reynolds number was carried out (Baroudi and Lee, 2021). The pressure fluctuation and velocity fluctuation are numerically studied during the bubble detachment (Cai et al., 2018). In an unsteady turbulence of the venturi bubble generator, the numerical simulation on the bubble dynamics is carried out (Song et al., 2021).

Most of the research studies on multiphase flow are based on water or other transparent viscous liquids, whereas it is hard to conduct experiments and visualize the bubbles in liquid metals such as molten LBE. The rising motion of single bubbles in the LBE pool is studied by neutron radiography (Hibiki et al., 2000), indicating that the migration behavior is similar to the typical characteristics of bubble migration in two-phase flow, and the results agree well with 1D and 2D simulations using the SIMMWE-III code. The bubble coalescence in the GaInSn eutectic alloy is investigated by X-ray photography (Keplinger et al., 2018). The rising velocity and the shape of small helium bubbles are indirectly measured by a layer of glycerol above the molten LBE pool (Konovalenko et al., 2017). The drag coefficient of single bubbles in molten LBE is obtained by analogy with several transparent liquids; then the prediction of the terminal rising velocity of single bubbles in molten LBE is carried out (Zhang et al., 2018). The diffusive interface method is applied for the 2D simulation of nitrogen single bubbles, and the results agree with Grace's graphical correlation (Wang and Cai, 2018). Nevertheless, the experimental research on the bubble migration behavior in molten LBE is restricted due to the opacity, and 2D simulation studies cannot completely describe the movements and forces of bubbles in three dimensions. Thus, the research on the bubble migration behavior in molten lead and bismuth is still insufficient.

In order to study the release and migration behavior of fission gas bubbles in the molten LBE pool of LFR, 3D numerical simulation based on the VOF method was carried out. The effects of gas injection velocity, release depth, and gas injection angle on the bubble release and migration behavior in molten LBE were

investigated. The bubble rising velocity, bubble equivalent diameter, and bubble detachment time, which are of great importance in bubble dynamics, were measured. The results were compared with theoretical analysis. This paper contributes to deepening the understanding of the mechanism of the release and migration behavior of fission gas bubbles in the molten LBE pool of LFR, and it provides a reference for system design optimization as well as safety analysis of LFR.

Numerical method

Governing equations

For incompressible fluids, the continuity equation and the momentum equation with surface tension are as follows:

$$\nabla.\vec{u} = 0 \tag{1}$$

$$\rho\left(\frac{\partial\vec{u}}{\partial t} + \left(\vec{u}.\nabla\right)\vec{u}\right) = -\nabla p + \nabla.\left(\mu\left(\nabla\vec{u} + \left(\nabla\vec{u}\right)^{T}\right)\right) + \rho\vec{g} + \vec{F_s} \tag{2}$$

where $\vec{u}$ denotes the fluid velocity, ρ denotes the density, p denotes the pressure, μ denotes the dynamic viscosity coefficient, $\vec{g}$ denotes the acceleration of gravity, and $\vec{F_s}$ denotes the equivalent body force of the surface tension. The system of Navier–Stokes equations consists of the continuity equation and the momentum equation.

The VOF method (Hirt and Nichols, 1981) is a free interface tracking method based on a fixed Euler grid, which has the advantages of a high efficiency and good precision. In this method, two or more immiscible fluids share a set of momentum equations, and the interface in the computational domain is tracked by the volume fraction C as follows:

$$\begin{cases} C = 0, & gas \\ 0 < C < 1, & interface \\ C = 1, & liquid \end{cases} \tag{3}$$

For the i^{th} phase, the volume fraction satisfies the volume fraction equation as follows:

$$\frac{\partial C_i}{\partial t} + \vec{u_i} \cdot \nabla C_i = 0 \tag{4}$$

In the current case, gas and liquid phases satisfy

$$\sum_{i=1}^{2} C_i = 0 \tag{5}$$

In the continuum surface force (CSF) model (Brackbill et al., 1992), with the divergence theorem, the surface tension at the interface can be expressed as an equivalent body force as follows:

$$F_S = \frac{\rho\sigma\kappa\nabla C_l}{0.5\left(\rho_g + \rho_l\right)} \tag{6}$$

where ρ is the density; g and l denote, respectively, the gas phase and liquid phase; σ denotes the surface tension coefficient; and κ denotes the interface curvature; the density and the viscosity are respectively obtained by the following scalar equations:

$$\rho\left(\vec{x},t\right) = \rho_l C\left(\vec{x},t\right) + \rho_g\left(1 - C\left(\vec{x},t\right)\right) \tag{7}$$

$$\mu\left(\vec{x},t\right) = \mu_l C\left(\vec{x},t\right) + \mu_g\left(1 - C\left(\vec{x},t\right)\right) \tag{8}$$

Boundary conditions and solution strategy

In this paper, the gas injection is divided into two modes: gas injection at the bottom orifice and gas injection at the wall orifice. As shown in Figure 1A, the simulation computational domain for the migration of bubbles continuously generated through ∇gas injection at the bottom orifice is a cuboid of 30 mm × 30 mm × 75 mm, and the orifice is located at the center of the bottom surface. In Figure 1B, when simulating the bubbles released by gas injection through the wall orifice, in order to further reduce the unnecessary computation, one of the dimensions of the bottom surface of the computational domain is shortened to 20 mm, and the height of the orifice is 10 mm. The orifices are 1 mm in diameter. The meshing of the entire computational domain is based on a structured mesh with a size of 0.5 mm. Since the shape of the orifice is circular, an O-grid is applied for the meshing. The processes of geometry and meshing were performed using ANSYS ICEM. The velocity inlet is set at the orifice. The top surface of the computational domain is set as the pressure outlet, and other surfaces are non-slip walls. The operation condition of the simulation is under an atmospheric pressure, that is, $1.013 \times 10^5\ Pa$. Initially, the liquid in the domain was in a static state.

In view of the huge difference in magnitude of physical properties such as density and viscosity between the gas and liquid, the volume of the bubble, which is affected by temperature, pressure, and physical properties, would be mainly concerned. Therefore, air is used as the general representative of the gas phase. At the same time, it is assumed that the effect of heat transfer between the bubble and the external fluid could be neglected. The physical properties of the studied fluids are given in Table 1.

The simulations are performed with ANSYS Fluent. The pressure-based and transient solver is selected. The gravity is $-9.81\ m/s^2$ in the z-direction. In the VOF model, the volume fraction discretization method is explicit, and the interface modeling is sharp. The CSF model is selected in the phase interaction section. The pressure–velocity coupling scheme is the Pressure-Implicit with Splitting of Operators (PISO) method, the pressure discretization method is PREssure STaggering Option (PRESTO), the momentum discretization method is the QUICK mode, and the volume

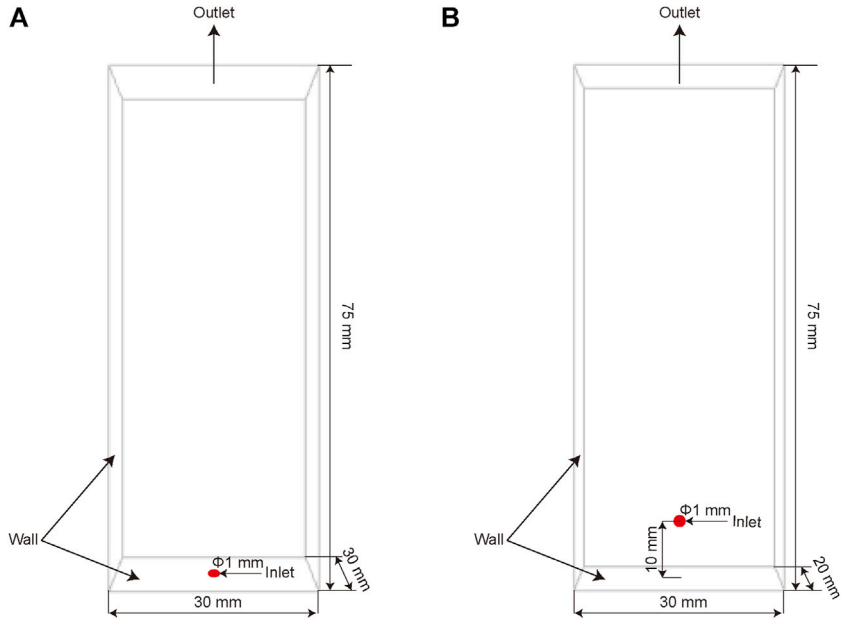

FIGURE 1
Schematic of the computational domain. **(A)** Bottom injection. **(B)** Wall injection.

TABLE 1 Material properties.

Material	Air	Water	LBE
Temperature (°C)	25	25	400
Density (kg/m^3)	1.225	998.2	10194.62
Viscosity (kg/m/s)	1.7894e-5	0.001003	0.001514
Surface tension (N/m)	—	0.0728	0.3947

TABLE 2 Detachment time and diameter of the first bubble in water when $v_g = 1\,m/s$.

Grid size (mm)	0.25	0.4	0.5	1.0
Total numbers of nodes	660,049–992,052	1,122,094	604,505	77,824
Detachment time (s)	0.110	0.100	0.100	0.135
Equivalent diameter (mm)	5.34	5.05	4.98	5.44

fraction discretization method is Geo-Reconstruct. Considering the calculation speed and convergence, the Courant number is controlled between 0.1 and 0.8; then the time step is adapted from 10^{-5} to 10^{-3} s, and the time interval of output data is 0.005 s.

The post-processing is conducted with CFD-Post. The bubble edge is defined by the iso-surface where the air bubble volume fraction is 0.4, and the acquisition of the data is based this iso-surface. The bubble's length, width, and height are measured; then the rising velocity and aspect ratio are calculated. The instantaneous rising velocity is defined as the average velocity calculated from the distance that the bubble rises in 0.005 s, while the terminal rising velocity is the average of the instantaneous rising velocity after the bubble has finished accelerating. The volume of the bubble is obtained by volume integration of the grids, and the equivalent diameter of the bubble is calculated from the bubble volume.

Grid independent test

In order to study the effect of mesh size on the simulation results, the grid-independent test is conducted through the simulation of bubbles released by gas injection in water. Air passes through the orifice with a diameter of 1 mm at the gas velocity of 1 m/s, and bubbles emerge, grow and detach from the orifice, and rise in the computational domain of a cuboid of 30 mm × 30 mm × 75 mm with grid sizes of 0.25, 0.4, 0.5, and 1.0 mm, respectively. In the computational domain, the overall mesh is based on structured meshes. The total numbers of nodes are given in Table 2, and it should be noted that the 0.25 mm grid is only applied near the gas–liquid interface.

Figure 2 shows the meshes before the first bubble detaches under grids of different sizes. It can be observed that the bubbles all show the shape of a rounded upper part and a shrinking neck shape before they are released. The finer the mesh is, the

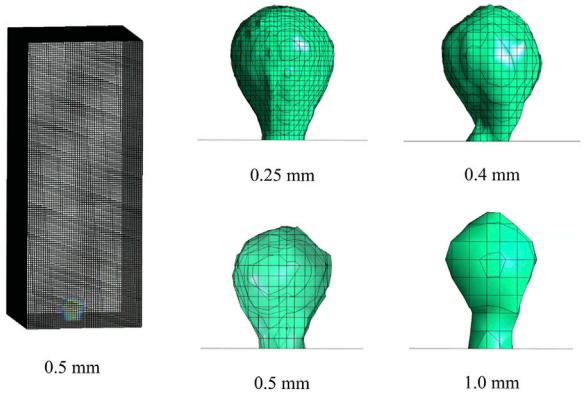

FIGURE 2
Mesh of the bubble before detachment with different grid sizes.

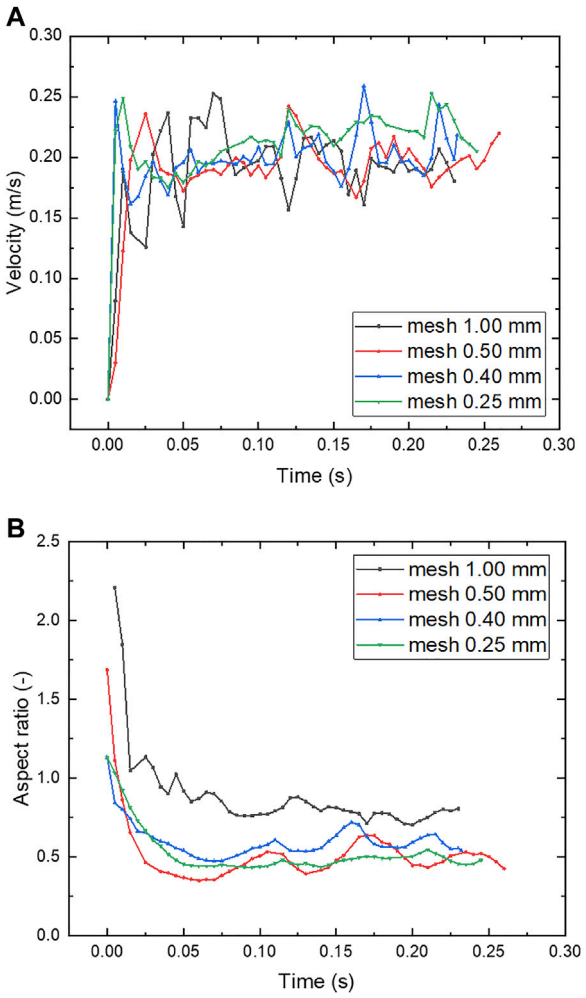

FIGURE 3
(A) Rising velocity and **(B)** aspect ratio of the bubble in water with different grid sizes, $v_g = 1\,m/s$.

smoother and rounder the bubble interface is described, and when the mesh is thicker, the surface of the bubble gradually appears angular, and the position of the bubble center is higher. The grid-independent analysis mainly focuses on the detachment time and size of the first bubble released from the orifice under different mesh sizes as well as the instantaneous rising velocity and aspect ratio of the bubble after the detachment.

The detachment time of the first bubble emerging from the orifice and the corresponding equivalent diameter are shown in Table 2. The detachment time and equivalent diameter of the first bubble in grids under 0.5 mm are close, and the detachment is obviously delayed in the grid of 1.0 mm. The rising velocity in different grids is shown in Figure 3A; similar behaviors are found where the rising velocity increases rapidly after the bubble detaches and then fluctuates within a certain range. Figure 3B shows that the aspect ratio drops rapidly and then fluctuates around a stable value. The results of grids under 0.5 mm are close, while the result with the 1.0 mm grid is sometimes unstable and the values of aspect ratio are generally higher.

The above simulations verify the independence of the grid and show that a grid size of 0.5 mm is sufficient to reasonably and accurately simulate and analyze the migration characteristics of bubbles in liquids. For a typical bubble with an equivalent diameter of 5 mm, the number of grids is about 500. Therefore, considering the rationality and accuracy of the calculation and taking into account the convergence and speed of the calculation, a grid with a size of 0.5 mm is used for the following 3D numerical simulations.

Model verification

Model verification is an indispensable part of numerical study. In order to verify the rationality and applicability of the model, the 3D simulation of a bubble released in water is conducted. A bubble with an equivalent diameter of 4 mm, which is found typical for the study of bubble migration in liquids, is released and rises under the action of buoyancy. The simulation of the bubble rising in water is compared to the experiment conducted in the laboratory of Sun Yat-Sen University, and the process of bubble rising in water was captured using a high-speed camera.

Simulation snapshots and experimental results of a 4 mm bubble rising in quiescent water are compared in Figure 4. It is found that the simulation results of the height, the deformation, and the motion of the bubble agree well with the experiment. After the bubble is released, the bottom of the bubble rapidly becomes flat, and the shape of the bubble becomes ellipsoidal. The rising trajectory of the bubble is zigzag on the 2D view, while it is flat and upward spiral in 3D

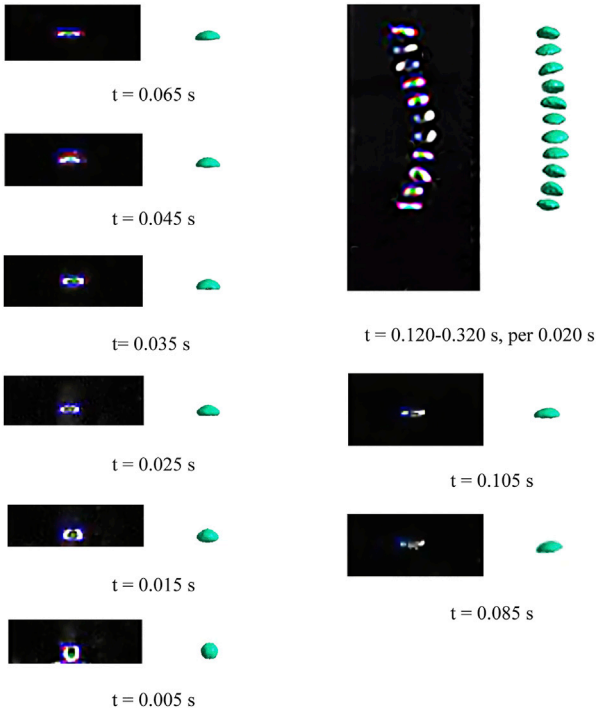

FIGURE 4
Comparison of experiments and 3D simulation of the bubble rising in water, $d = 4\,mm$.

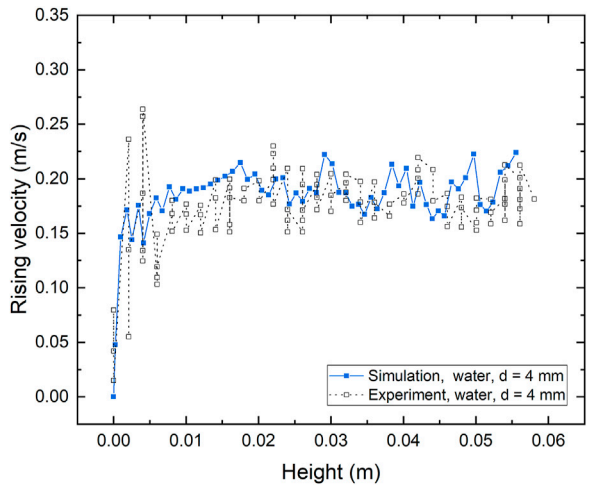

FIGURE 5
Comparison of 3D simulation and experiments of bubble rising velocity with height in water.

FIGURE 6
Snapshots of 3D simulation of bubbles released by gas injection in molten LBE, $v_g = 1\,m/s$.

view. The wobble of the bubble has a similar direction in simulation and experiments, but the deviation is less important in simulation. Due to the purity of the fluid and the actual situation of the field, the difference between simulation and experiments is inevitable. It is hard to make sure that the liquid is absolutely quiescent in experiments, and the gas velocity and pressure will affect the result, which lead to the motion of the bubble in experiments being more violent. Generally, the result of simulation agrees well with experiments.

Figure 5 shows the rising velocities of a 4 mm bubble in water with height in simulation as well as in experiments. The rising velocities increase rapidly once the bubbles are released and then fluctuate within certain ranges. The results in simulation and in experiments are similar and comparable. Considering the complexity of the bubble migration behavior, the agreement between simulation and experimental results of the bubble in water is acceptable, which indicates that the methodology is reasonable and feasible to study the bubble migration behavior in the liquid, and the modifications in material properties from water to molten LBE would be possible. Hence, this model can be applied to the study on the bubble migration behavior in molten LBE.

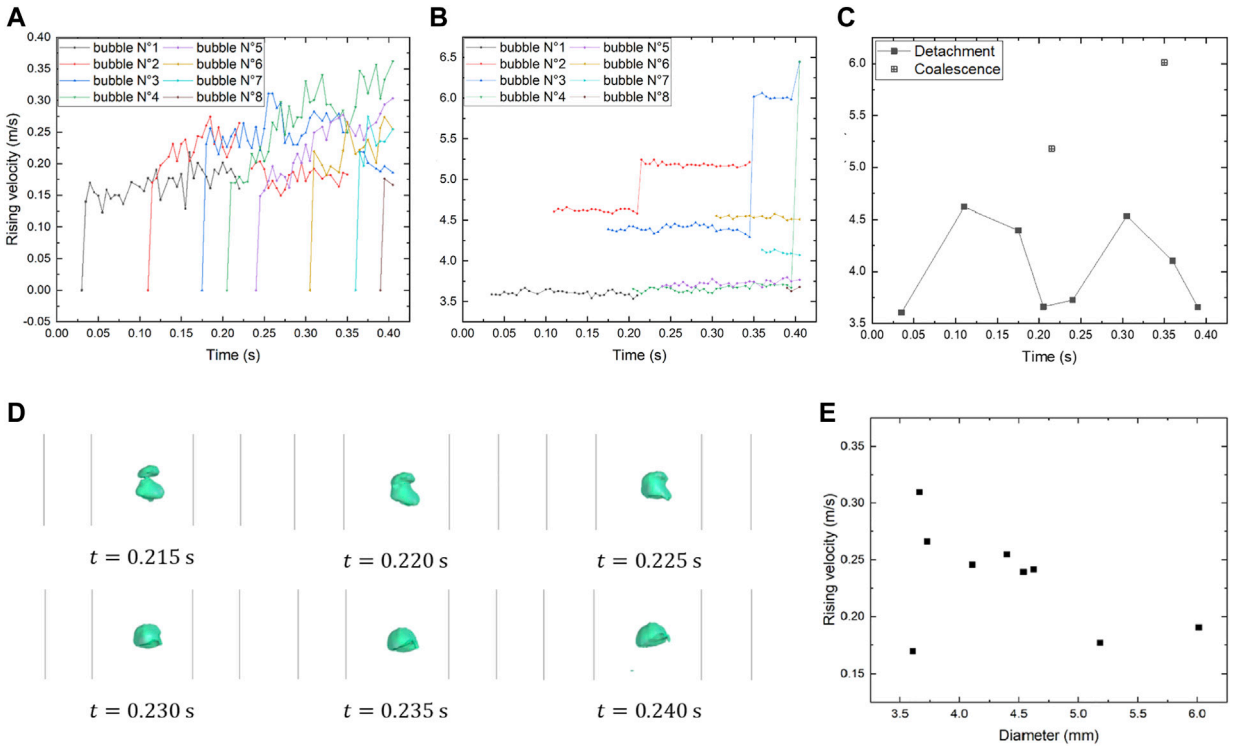

FIGURE 7
Simulation results of bubbles released by gas injection in molten LBE, $v_g = 1\,m/s$. **(A)** Rising velocity. **(B)** Equivalent diameters. **(C)** Detachment and coalescence. **(D)** Coalescence of bubbles No. 1 and 2. **(E)** Terminal rising velocity.

Results and discussion

Bubbles released by gas injection in the molten lead–bismuth eutectic

In a postulated severe accident in LFR, the damage of the fuel rods could cause the ejection of the high-pressure fission gas contained within and thereby generate bubbles. In order to better understand the release and migration behavior of fission gas bubbles in molten LBE pools under severe accidents, a 3D numerical study of bubble migration behavior under the condition that gas bubbles are continuously generated by gas injection is carried out in this part. At the same time, in order to study the potential influencing factors of bubble migration behavior in the postulated severe accident of LFR, the effects of different parameters including gas injection velocity, release depth, and gas injection angle were studied. The results of the bubble rising velocity, bubble detachment time, and bubble equivalent diameter were measured.

Figure 6 shows the snapshots of 3D simulation of bubbles continuously generated at a gas injection velocity $v_g = 1\,m/s$ through the orifice with a diameter of 1 mm at the bottom of the computational domain. The bubbles undergo the generation, growth, and detachment. Then, the bubbles float upward in the computational domain under the action of inertia and buoyancy. After the bubbles detach from the orifice, the lower surface quickly becomes flat or even concave and then becomes hemispherical or ellipsoidal, and the bubbles rise with wobbling. Within 0.4 s of the simulation, eight bubbles have detached at the orifice, which are named bubble No. 1 to bubble No. 8 according to the detachment order. Figure 7A shows the instantaneous rising velocities of these bubbles. It is observed that the bubbles continuously generated by gas injection in molten LBE have typical bubble rising characteristics; that is, the rising velocities of the bubbles first increase rapidly after detaching at the orifice and then fluctuate around stable values.

Under the current conditions, the coalescence of bubbles can be clearly observed. The coalescence of bubble No. 1 and No. 2, the coalescence of bubble of No. 2 and No. 3, and the coalescence of bubble of No. 3 and No. 4 occurred at 0.215, 0.350, and 0.405 s, respectively, forming a bigger bubble at each time. It is found in Figure 7B that the equivalent diameter of the bubbles remains basically stable during the rising process except during the coalescence process. Among them, the bubbles with a too short simulation duration were not analyzed. It can be seen in Figure 7C that at the gas injection velocity $v_g = 1\,m/s$, the equivalent diameter of the bubbles has a certain periodicity. The equivalent diameter of the bubbles detaching from the

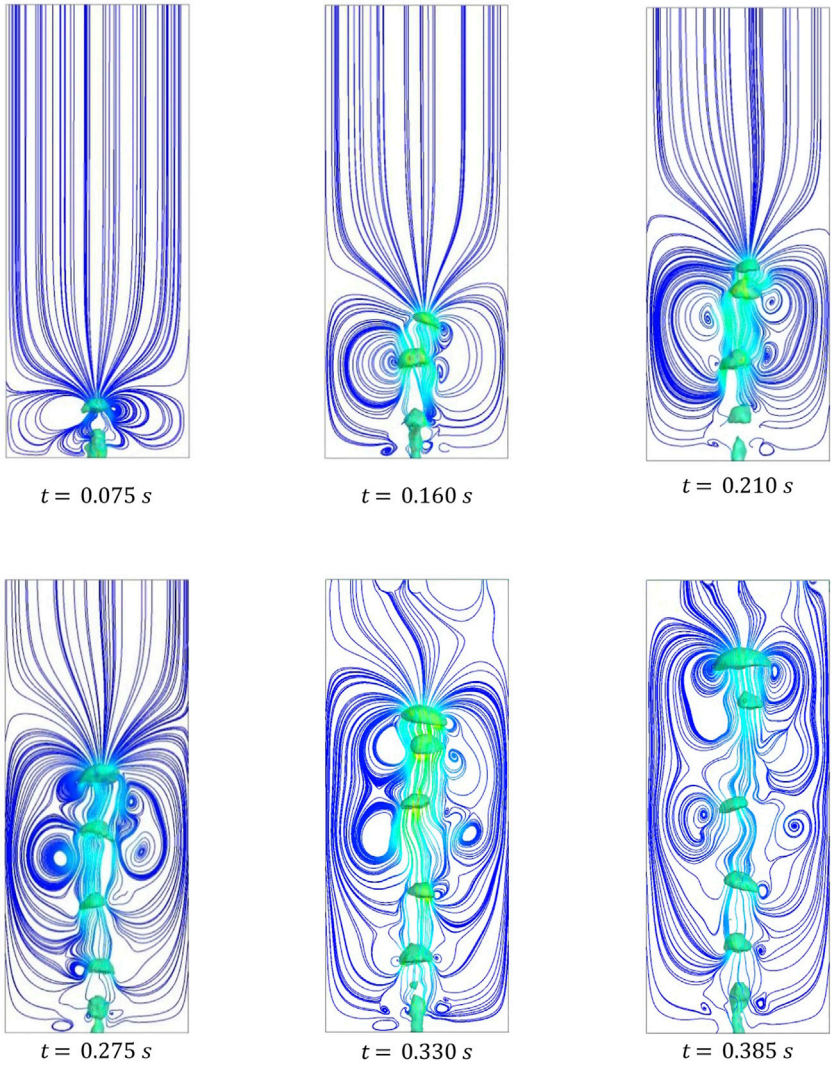

FIGURE 8
Streamlines of the velocity field of bubbles released by gas injection in molten LBE, $v_g = 1\,m/s$.

orifice is between 3.5 and 4.6 mm, and the fluctuation period of its value is about 0.2 s. The frequency of releasing bubbles is 0.049, and the equivalent diameters of the bubbles after coalescence are all greater than 5 mm.

Figure 7D shows the process of coalescence of bubble No. 1 and bubbles No. 2. The leading bubble usually has a lower rising velocity, and due to the effect of the wake of the leading bubble, the trailing bubble is accelerated and its top surface extends to reach the leading bubble's lower surface and then eventually merges with the leading bubble. The coalescence of bubbles leads to the formation of a bigger bubble. This phenomenon is also found in the study of Hasan (Hasan and Zakaria, 2011). It can be seen in Figure 7A that the rising velocity of the bubble after coalescence is slightly higher than the leading bubble.

Figure 8 shows the streamlines of the velocity field during the release and rising of bubbles. It is observed that the streamlines around the first bubble have good symmetry and the field above is tranquil. While it is found that the bubble wake has a long distance and straight impact on the bubbles down below, most of the bubbles detaching afterward get in the wake of the upper bubbles. The bubbles in the wake not only are accelerated but also could be deviated horizontally. With the continuous release and rising of bubbles, the streamlines become more complex but maintain a relatively good symmetry, which keeps the bubbles being influenced by the bubble wake.

Therefore, it can be seen in Figure 7E that no simple or linear relationship exists for the terminal rising velocity of bubbles released by gas injection in molten LBE and it is divided into two cases. One of the cases is the bubbles not being influenced by the

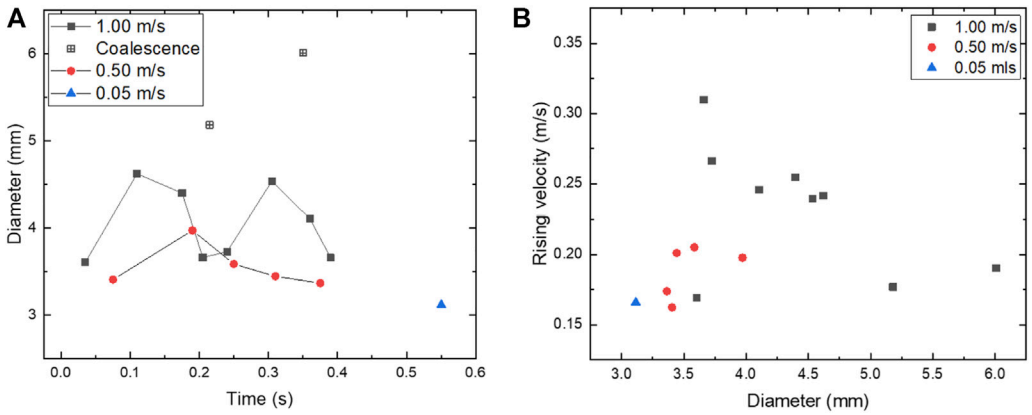

FIGURE 9
Effect of gas injection velocity on the release and migration behavior of bubbles in molten LBE. **(A)** Equivalent diameter. **(B)** Terminal rising velocity.

bubble wake, and the other is the bubbles influenced by the bubble wake. The first bubble detaching at the orifice and the bubbles after merging with it are not influenced by the wake, and their terminal rising velocities are lower than 0.20 m/s, as shown in Figure 7E, and only after the coalescence, the rising velocity increases slightly. While the bubbles get influenced by the wake of the upper bubble, the wake causes the decrease of the pressure, the increase of fluid velocity, and the formation of vortexes. These differences in the flow field accelerate the bubbles that are in the wake, making their terminal rising velocities greater than 0.20 m/s.

Effect of gas injection velocity

In order to study the effect of gas injection velocity on the bubble migration behavior, the simulations were conducted under the condition of gas injection though the orifice at the bottom surface of the computational domain, with the typical gas injection velocity $v_g = 1m/s$, $0.5m/s$, $0.05\,m/s$. It is found that the gas injection velocity has a great impact on the number of bubbles and the detachment time. Moreover, the coalescence of bubbles is found when $v_g = 1m/s$, while it is not observed when $v_g = 0.5m/s$ and $v_g = 0.05m/s$.

The detachment time and equivalent diameter of bubbles in molten LBE at each gas injection velocity are shown in Figure 9A, where the coalescence of bubbles occurs at $v_g = 1m/s$. Reducing the gas injection velocity can significantly delay the detachment time. At a smaller gas injection velocity, the equivalent diameter of the bubble is smaller when the bubble detaches at the orifice. For example, when $v_g = 1m/s$, the range of equivalent diameters of the bubble is 3.6–4.6 mm, and it increases with the coalescence of bubbles, while when $v_g = 0.5m/s$, the range of equivalent diameters of the bubble reduces to 3.4–4.0 mm; when $v_g = 0.05m/s$, only one bubble with an equivalent diameter of 3.1 mm is released. It is observed that the equivalent diameter of the first bubble increases slightly with the increase of gas injection velocity. However, there is no obvious difference in the terminal rising velocity.

Figure 9B shows the distribution of bubble terminal rising velocity with equivalent diameter at the gas injection velocities of $v_g = 1m/s$, $0.5m/s$, $0.05\,m/s$. There is no simple and linear relationship existing, and there are two zones when $d \leq 4.5\,mm$: one of the zones when $3.5\,mm \leq d \leq 4.5\,mm$, where the terminal rising velocity drops from 0.31 m/s to 0.24 m/s, and the other when $3.0\,mm \leq d \leq 4.0\,mm$, where the terminal rising velocity increases from 0.16 m/s to 0.20 m/s. When $d > 4.5\,mm$, the terminal rising velocity is around 0.18 m/s. For the first bubble detaching at the orifice and the bubbles after merging with the first bubble, they are less likely to be affected by the bubble wake, and the flow field above these bubbles is tranquil and quiescent. Therefore, these bubbles are not obviously accelerated and their terminal rising velocities are relatively low. However, the bubbles that are greatly affected by the wake of the upper bubble will accelerate. At a higher gas injection velocity, the time between bubbles leaving the orifice is shorter, and there is a greater chance of entering the wake of the upper bubble, so it is easier to be accelerated. For example, when $v_g = 1m/s$, the terminal rising velocity can be accelerated up to 0.30 m/s. At a lower gas injection velocity, the time between bubble detachments prolongs, weakening the influence of the wake between bubbles, so the bubbles are less accelerated. When $v_g = 0.5m/s$, the terminal rising velocity can be accelerated up to 0.20 m/s. When $v_g = 0.05m/s$, the second bubble does not detach when the first bubble leaves the computational domain and the effect of the wake could be neglected.

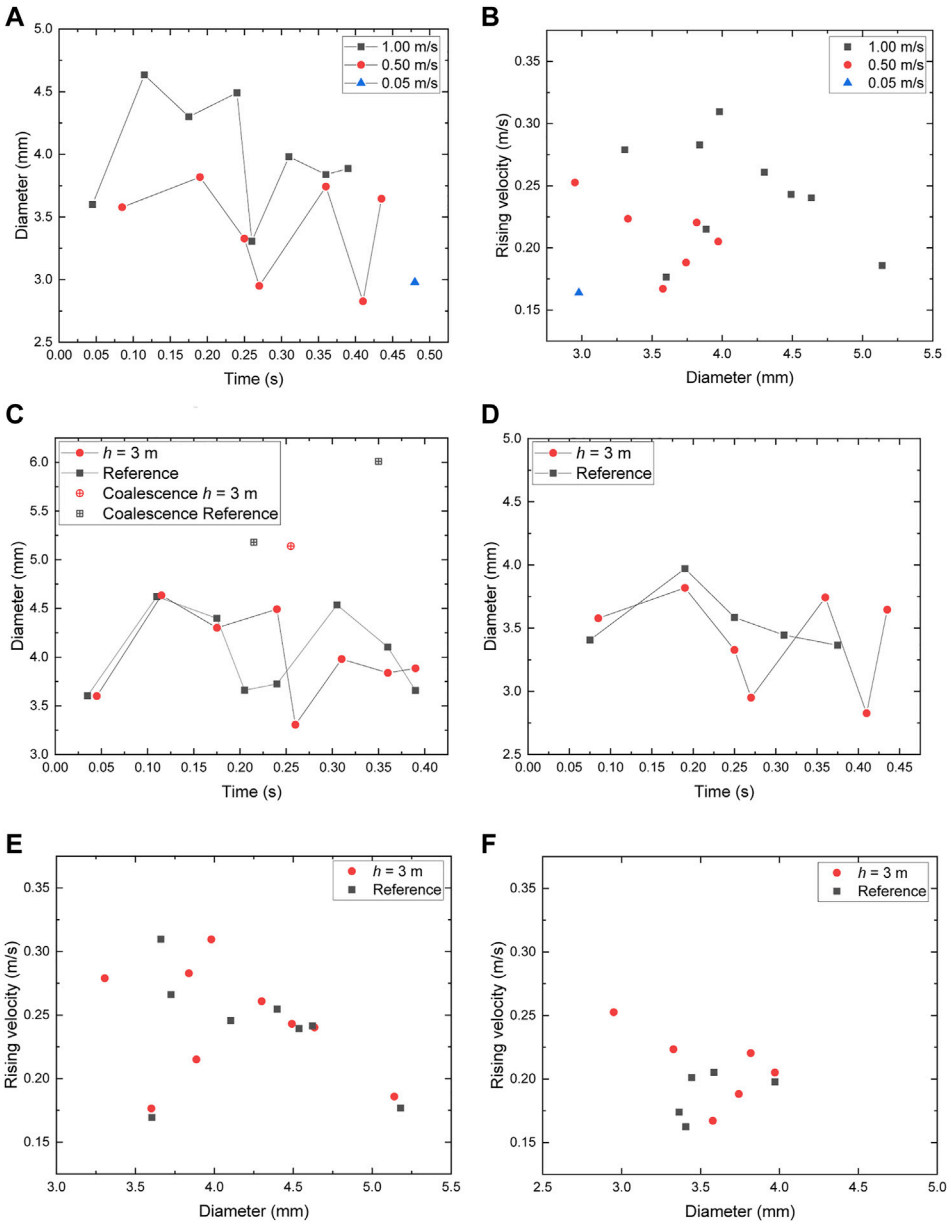

FIGURE 10
Influence of release depth on the release and migration behavior of bubbles in molten LBE. **(A)** Equivalent diameter. **(B)** Terminal rising velocity. **(C)** Equivalent diameter, v_o = 1 m/s. **(D)** Equivalent diameter, v_o = 0.5 m/s. **(E)** Terminal rising velocity, v_o = 1 m/s. **(F)** Terminal rising velocity, v_o = 0.5 m/s.

Effect of release depth

In order to study the effect of release depth on the bubble migration behavior in molten LBE, a layer of molten LBE of 3 m is added above the computational domain. Due to the limitation of computing resources, it is not possible to directly lengthen the computational domain by 3 m. Instead, the change in the length of the computational domain is equivalent by increasing the back pressure at the pressure outlet. The back pressure of $p_b = 0.3\ MPa$ is applied to the pressure outlet, which is equivalent to adding molten LBE with a thickness of 3 m above the computational domain, and the position of the orifice is equivalent to the lower middle position of the molten LBE pool. Studying the effect of release depth helps to better simulate the conditions of bubbles in the melt pool of LFR.

Simulations were carried out with the increase of release depth $h = 3\,m$ at the gas injection velocities of $v_g = 1m/s$, $0.5m/s$, $0.05\,m/s$. It is found in Figure 10A that the decrease of the gas injection velocity also causes the delay of detachment time and the decrease of the equivalent diameter, which is the same as the effect of the gas injection velocity without the increase of the depth.

Figures 10C,D show the influence of release depth on the detachment time and equivalent diameter of bubbles at $v_g = 1m/s$ and $v_g = 0.5m/s$. Only slight delay in the detachment is found after increasing the release depth, while the equivalent diameter of the bubble varies more violently at each detachment, and the coalescence of bubbles is also delayed when $v_g = 1m/s$. Moreover, when $h = 3\,m$ and $v_g = 1m/s$, the range of equivalent diameters shrinks from 3.6–4.6 mm to 3.3–4.6 mm, and for $v_g = 0.5m/s$, this range turns from 3.4–4.0 mm to 2.9–4.0 mm. This result indicates that the increase of release depth tends to reduce the lower limit of the range of equivalent diameters of the bubble released. Similarly, when $v_g = 0.05m/s$, the increase of depth turns out the decrease of the size of bubbles by about 1%. However, the gas volume of the bubble reduces and the detachment is in advance.

Figure 10B shows the distribution of bubble terminal rising velocity with equivalent diameter when $h = 3\,m$ at different gas injection velocities, and two zones of the terminal rising velocity are also observed. It infers that the bubbles with lower terminal rising velocities are less influenced by the bubble wake, while the bubbles with higher terminal rising velocities are accelerated by the wake of the upper bubbles. When the gas injection velocity decreases, the equivalent diameter of the bubble decreases, and the distance between bubbles extends at the same time, weakening the acceleration effect of the bubble wake. With the decrease of gas injection velocity, the distribution map of terminal rising velocity moves to the bottom left as a whole and finally gets gathered at the bottom left at a very low gas injection velocity. After the increase of release depth, the distribution is more dispersed than that in Figure 9B.

Figures 10E,F show the effect of release depth on the distribution of bubble terminal rising velocity with equivalent diameter at $v_g = 1m/s$ and $v_g = 0.5m/s$. At the gas injection velocity of 1 m/s, the difference of the distribution is not obvious by the change of release depth: when the equivalent diameter is greater than 4 mm, the terminal rising velocity decreases; when the equivalent diameter is below 4 mm, the terminal rising velocity is divided into a higher branch and a lower branch. At the gas injection velocity of 0.5 m/s, the bubbles are smaller than 4 mm, and the bubbles with an equivalent diameter of 3.4–4.0 mm have close terminal rising velocities before and after the increase of release depth. The increase of release depth can cause the generation of smaller bubbles within a shorter duration, making these bubbles more easily accelerated by the wake of the upper bubble.

Effect of gas injection angle

In the reactor, the fuel rods are in a vertical position. Under a postulated severe accident, the damage could happen on a vertical surface, in which the shear force applied on the bubble would be different. Hence, the gas injection angle is to be studied. The orifice with a diameter of 1 mm is located on the midline of a vertical wall, and the distance to the bottom surface is 10 mm. The gas injection velocities of 1 m/s, 0.5 m/s, and 0.05 m/s are applied.

Figure 11 shows the snapshots of simulation of the bubbles generated by gas injection at the wall orifice in molten LBE. It can be observed that the bubbles released at the wall orifice will rise and attach to the wall. The bubbles with a large gas volume tend to form half-cut bubbles, while the bubbles with a smaller gas volume tend to form gas films and the tiny bubbles on the wall surface. Compared to the previous cases where the orifice is on the bottom surface, more bubbles are generated at the orifice on the wall, and the bubbles that attach to the wall are more favorable to the coalescence of bubbles.

Figure 12A shows the instantaneous rising velocities of bubbles numbered by the order of detachment when $v_g = 1\,m/s$. There are nine bubbles released within 0.335 s, indicating that the bubbling frequency is higher than previous cases. The instantaneous rising velocity of the bubble is similar to those of the bubbles released at the orifice on the bottom surface; that is, the rising velocity of the bubble accelerates at the beginning and then fluctuates within a certain range. The bubbles attaching to the wall generally have higher rising velocities because of the guidance of the wall. Before the coalescence of bubbles, the wake of the upper bubble has an acceleration effect on the bubble below so that the bubble can reach a higher instantaneous rising velocity. The breakpoint of the curve in Figure 12A indicates the coalescence of bubbles. It is observed that the instantaneous rising velocity of the bubble after coalescence is lower than that of the trailing bubble and slightly higher than that of the original leading bubble. At the same time, it is found that sometimes, the phenomenon of bubble coalescence occurs the very moment after a bubble is just released from the orifice. For example, after bubble No. 5 is separated from the orifice, it accelerates to a high rising velocity so that it merges quickly with bubble No. 4.

The detachment time and equivalent diameter of bubbles generated by gas injection at the wall orifice in molten LBE at the gas injection velocities of 1 m/s and 0.5 m/s are shown in Figures 12C,D. The first bubble released at the orifice takes a longer waiting time than the rest of the bubbles, and therefore, more gas is accumulated to form a bigger bubble. Meanwhile, the flow field for the first bubble is tranquil, so its rising velocity is relatively low. The rest of the bubbles are smaller, and the time intervals between the bubble detachments are shorter; then these bubbles have short distances with each other. Therefore, theses bubbles are more easily accelerated under the effect of the wake of upper

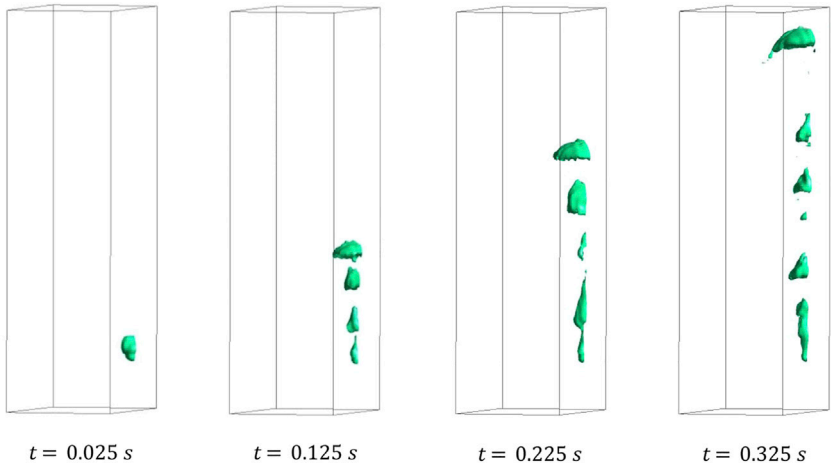

FIGURE 11
Snapshots of simulation of the bubbles generated by gas injection at the wall orifice in molten LBE, $v_g = 1\,m/s$.

bubbles and the coalescence of bubbles is facilitated. It should be noted that some of the bubbles merge right after their detachment with tiny bubbles, which detach almost at the same time, or with the gas column underneath, such as bubble No. 5 when $v_g = 1m/s$, and it is not shown in Figure 12C.

Figure 12B shows the detachment time and equivalent diameter at different gas injection velocities at the wall orifice. Compared with the results of the bubbles released at the orifice on the bottom surface in Figure 9A, it is found that bubbles are more easily released at the wall orifice and the bubbles are smaller. When $v_g = 1\,m/s$, the range of equivalent diameters decreases from 3.6–4.6 mm to 2.9–4.5 mm; when $v_g = 0.5\,m/s$, the range of equivalent diameters decreases from 3.4–4.0 mm to 2.0–3.4 mm; when $v_g = 0.05\,m/s$, the equivalent diameter drops from 3.1 mm to about 1.9 mm. The decrease of gas injection velocity delays the detachment time and the number of bubbles. In addition, the equivalent diameter decreases, and the fluctuation of the bubble equivalent diameter is less violent.

Figure 12E shows the distribution of terminal rising velocity with equivalent diameter of the bubbles generated by gas injection at the wall orifice in molten LBE. The existence of two zones which depend on the influence of the bubble wake is observed referring to the previous cases. Most of the small bubbles tend to chase after bigger bubbles; then these small bubbles are accelerated and reach higher rising velocities. The bubbles with larger diameters usually formed after merging with other bubbles, and their terminal rising velocities maintain around 0.20 m/s. With the decrease in the gas injection velocity, the equivalent diameter of the bubble decreases, and the terminal rising velocity decreases, which is equivalent to moving the overall distribution to the bottom left. Finally, when the gas injection velocity is very low, the data point converges at the bottom left of the diagram. Compared with Figure 9B, the terminal rising velocity of the bubble released by the wall orifice is generally higher than that of the bubble released by the orifice on the bottom surface.

Theoretical analysis

Numerical simulation provides a more economical and feasible path for more difficult and complex experimental research, especially for the molten LBE of opaque and complicated operations to carry out general experimental research. However, in order to discuss the rationality and accuracy of numerical simulation results, it is still useful to compare the results of numerical simulation with theoretical analysis.

Grace's graphical empirical correlation (Clift et al., 1987) describes the shape and rising characteristics of the bubble by the dimensionless numbers, namely, the Reynolds number (Re), Morton number (Mo), and Eötvös number (Eo), as follows:

$$Re = \frac{\rho_l U d}{\mu_l} \tag{9}$$

$$Mo = \frac{g\mu_l^4}{\rho_l \sigma^3} \tag{10}$$

$$Eo = \frac{\rho_l g d^2}{\sigma} \tag{11}$$

where the subscript l denotes the liquid phase, σ denotes the surface tension coefficient, d denotes the equivalent diameter of the bubble, μ denotes the dynamic viscosity coefficient, U denotes the rising velocity of the bubble, and g denotes the acceleration of gravity.

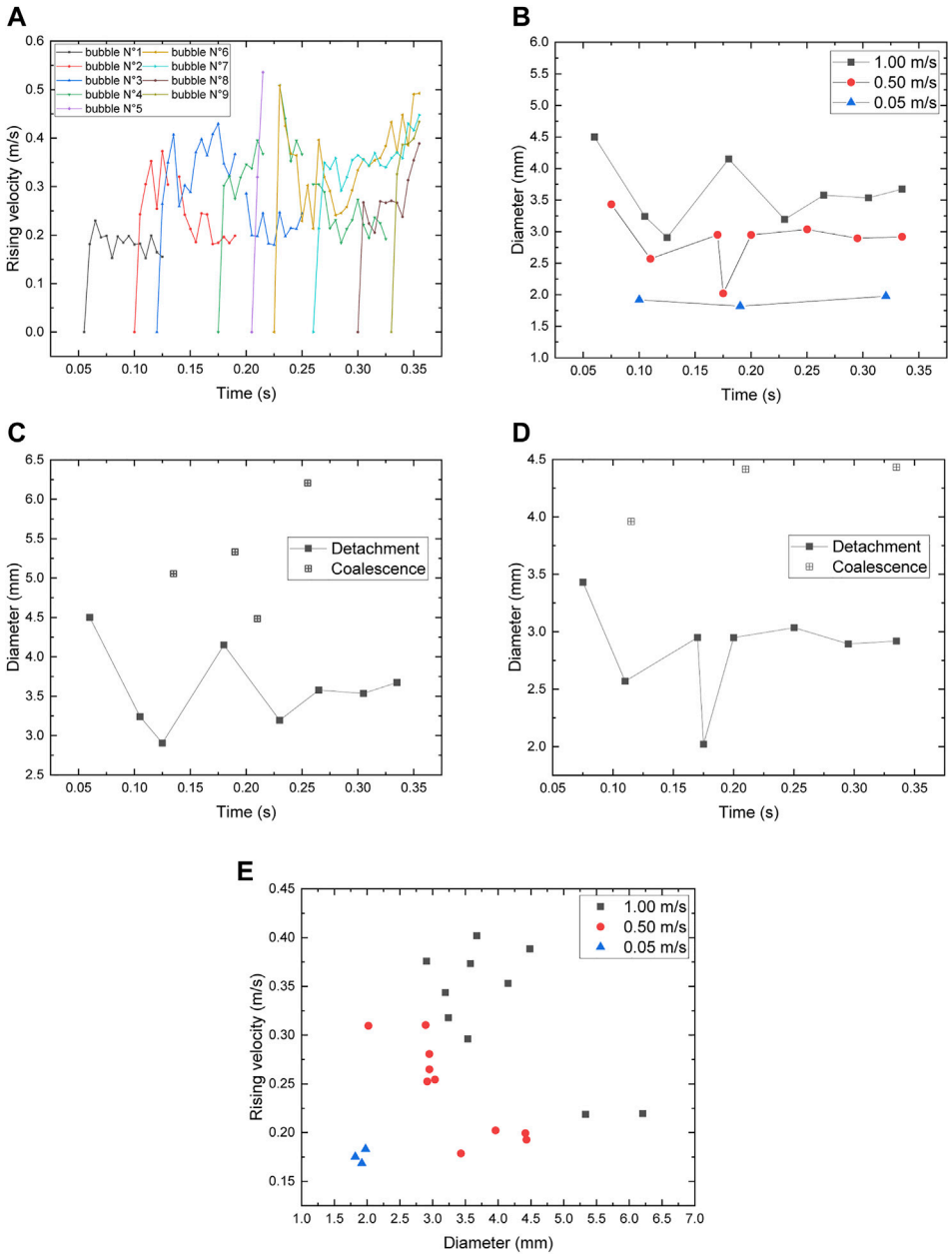

FIGURE 12
Release and migration behavior the bubbles generated by gas injection at the wall orifice in molten LBE. **(A)** Instantaneous rising velocity. **(B)** Equivalent diameter. **(C)** Equivalent diameter, v_o = 1 m/s. **(D)** Equivalent diameter, v_o = 0.5 m/s. **(E)** Terminal rising velocity.

Grace did not provide the curves at an extreme density ratio. The ranges of the dimensionless numbers including *Mo*, *Re*, and *Eo* are respectively 8.2×10^{-14}, $2.1 \times 10^{3} - 1.1 \times 10^{4}$, and 0.8 – 10. The high density and low viscosity of molten LBE result in the extreme situation of a high Reynolds number and a low Morton number. Therefore, the simulation results are located at the blank area of Figure 13, but the points tend to distribute with a similar tendency to the closest curve, where the Reynolds number increases with the Eötvös number. In addition, the shape of the bubbles is generally ellipsoidal with wobble, which agrees with the description of the bubbles located in the nearby region. The results of the cases of gas injection velocity and release depth almost have the same distributions. However, the distribution of the case of the wall orifice is wider and higher due a larger range of bubble sizes and a higher bubble terminal rising velocity. Hence, Grace's graphical empirical correlation

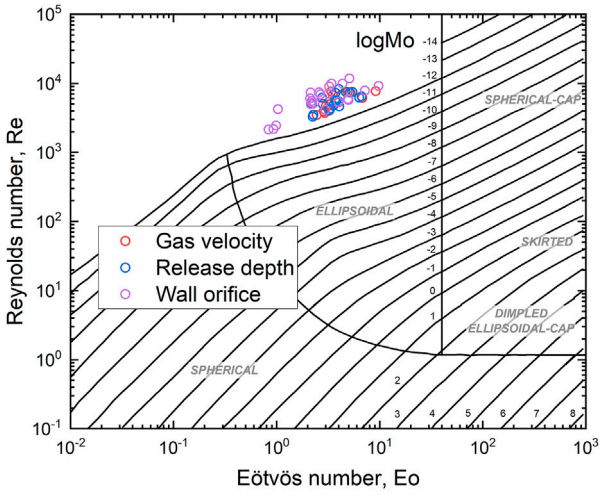

FIGURE 13
Simulation results on Grace's graphical empirical correlation.

and the results of simulation are still comparable, and it may be possible to predict the migration behavior of the bubbles in molten LBE, such as bubble shape and terminal rising velocity, by completing Grace's graphical empirical correlation at a higher Reynolds number.

Conclusion

In this paper, a 3D numerical study on the release and migration behavior of the fission gas bubbles in the molten LBE pool of LFR is carried out based on the VOF method. The acceleration effect of the wake of the upper bubble is confirmed, and coalescence of bubbles could be facilitated. The distribution of the terminal rising velocity with equivalent diameter of the bubble has no simple and linear relationship, and it depends on the influence of bubble wake. Decreasing the gas injection velocity delays the detachment time, decreases the bubbling frequency, and releases smaller bubbles. The increase of release depth tends to decrease the lower limit of the range of the bubble equivalent diameters, and the variation of bubble size may be more intense. The bubbles released at the orifice on the wall would reach higher rising velocities under the guidance of the wall and the acceleration effect of the bubble wake. The results of simulation are still comparable to Grace's graphical empirical correlation at the area of a higher Reynolds number, and the distribution of the terminal rising velocity with equivalent diameter may predict the migration characteristics of the bubbles in molten LBE. This paper contributes to deepening the understanding of the mechanism of the release and migration behavior of fission gas bubbles in the molten LBE pool of LFR and provides references for the system design optimization and safety analysis of LFR.

Data availability statement

The raw data supporting the conclusion of this article will be made available by the authors, without undue reservation.

Author contributions

ZM performed the investigation, analysis, and the writing of the first draft of the manuscript. HC wrote and edited sections of the manuscript. All authors contributed to manuscript revision, read, and approved the submitted version.

Funding

The research is funded by the Science and Technology Program of Guangdong Province (No. 2021A0505030026), the China Postdoctoral Science Foundation (No. 2019M663128), and the Basic and Applied Basic Research Foundation of Guangdong province (No. 2021A1515010343, No. 2022A1515011582).

Conflict of interest

ZZ was employed by China Nuclear Power Technology Research Institute Co., Ltd.

The remaining authors declare that the research was conducted in the absence of any commercial or financial relationships that could be construed as a potential conflict of interest.

Publisher's note

References

Baroudi, L., and Lee, T. (2021). Simulation of a bubble rising at high Reynolds number with mass-conserving finite element lattice Boltzmann method. *Comput. Fluids* 220, 104883. doi:10.1016/j.compfluid.2021.104883

Bhaga, D., and Weber, M. E. (1981). Bubbles in viscous liquids: Shapes, wakes and velocities. *J. Fluid Mech.* 105, 61–85. doi:10.1017/s002211208100311x

Brackbill, J. U., Kothe, D. B., and Zemach, C. (1992). A continuum method for modeling surface tension. *J. Comput. Phys.* 100, 335–354. doi:10.1016/0021-9991(92)90240-y

Cai, K., Song, Y., Li, J., Wang, D., Yin, J., Liu, W., et al. (2018). Pressure and velocity fluctuation in the numerical simulation of bubble detachment in a venturi-type bubble generator. *Nucl. Technol.* 205, 94–103. doi:10.1080/00295450.2018.1479575

Cinotti, L., Smith, C. F., and Sekimoto, H. (2009). *Lead-cooled fast reactor (LFR) overview and perspectives*. Livermore, CA, United States: Lawrence Livermore National Lab. LLNL.

Clift, R., Grace, J. R., and Weber, M. E. (1987). *Bubbles, drops, and particles*. New York: Academic Press.

Davies, R. M., and Taylor, G. I. (1950). The mechanics of large bubbles rising through liquids in tubes. *Proc. R. Soc. Lond. A* 200, 375–390.

Fazio, C., Sobolev, V. P., Aerts, A., Gavrilov, S., Lambrinou, K., Schuurmans, P., et al. (2015). *Handbook on lead-bismuth eutectic alloy and lead properties, materials compatibility, thermal-hydraulics and technologies-2015 edition*. Issy-les-Moulineaux, France: Organisation for Economic Co-Operation and Development.

Hasan, N., and Zakaria, Z. B. (2011). Computational approach for a pair of bubble coalescence process. *Int. J. Heat Fluid Flow* 32, 755–761. doi:10.1016/j.ijheatfluidflow.2011.02.004

Hibiki, T., Saito, Y., Mishima, K., Tobita, Y., Konishi, K., Matsubayashi, M., et al. (2000). Study on flow characteristics in gas-molten metal mixture pool. *Nucl. Eng. Des.* 196, 233–245. doi:10.1016/s0029-5493(99)00293-9

Hirt, C. W., and Nichols, B. D. (1981). Volume of fluid (VOF) method for the dynamics of free boundaries. *J. Comput. Phys.* 39, 201–225. doi:10.1016/0021-9991(81)90145-5

Joseph, D. D. (2003). Rise velocity of a spherical cap bubble. *J. Fluid Mech.* 488, 213–223. doi:10.1017/s0022112003004968

Kang, I. S., and Leal, L. G. (1988b). Small-amplitude perturbations of shape for a nearly spherical bubble in an inviscid straining flow (steady shapes and oscillatory motion). *J. Fluid Mech.* 187, 231–266. doi:10.1017/s0022112088000412

Kang, I. S., and Leal, L. G. (1988a). The drag coefficient for a spherical bubble in a uniform streaming flow. *Phys. Fluids (1994).* 31, 233–237. doi:10.1063/1.866852

Kelly, J. E. (2014). Generation IV international forum: A decade of progress through international cooperation. *Prog. Nucl. Energy* 77, 240–246. doi:10.1016/j.pnucene.2014.02.010

Keplinger, O., Shevchenko, N., and Eckert, S. (2018). Visualization of bubble coalescence in bubble chains rising in a liquid metal. *Int. J. Multiph. Flow* 105, 159–169. doi:10.1016/j.ijmultiphaseflow.2018.04.001

Konovalenko, A., Sköld, P., Kudinov, P., Bechta, S., and Grishchenko, D. (2017). Controllable generation of a submillimeter single bubble in molten metal using a low-pressure macrosized cavity. *Metall. Materi. Trans. B* 48, 1064–1072. doi:10.1007/s11663-017-0914-z

Mendelson, H. D. (1967). The prediction of bubble terminal velocities from wave theory. *AIChE J.* 13, 250–253. doi:10.1002/aic.690130213

Pioro, I. (2016). *Handbook of generation IV nuclear reactors*. Duxford, United Kingdom: Woodhead Publishing.

Plesset, M. S., and Chapman, R. B. (1971). Collapse of an initially spherical vapour cavity in the neighbourhood of a solid boundary. *J. Fluid Mech.* 47, 283–290. doi:10.1017/s0022112071001058

Prosperetti, A. (1977). Viscous effects on perturbed spherical flows. *Q. Appl. Math.* 34, 339–352. doi:10.1090/qam/99652

Rayleigh, L. (1917). VIII. On the pressure developed in a liquid during the collapse of a spherical cavity. *Lond. Edinb. Dublin Philos. Mag. J. Sci.* 34, 94–98. doi:10.1080/14786440808635681

Song, Y., Xu, R., Cai, K., Yin, J., and Wang, D. (2021). Numerical studies on bubble dynamics in an unsteady turbulence of the venturi bubble generator applied to TMSR. *Ann. Nucl. Energy* 160, 108322. doi:10.1016/j.anucene.2021.108322

Tomiyama, A., Celata, G., Hosokawa, S., and Yoshida, S. (2002). Terminal velocity of single bubbles in surface tension force dominant regime. *Int. J. Multiph. flow* 28, 1497–1519. doi:10.1016/s0301-9322(02)00032-0

Tomiyama, A., Kataoka, I., Zun, I., and Sakaguchi, T. (1998). Drag coefficients of single bubbles under normal and micro gravity conditions. *JSME Int. J. Ser. B Fluids. Therm. Eng.* 41, 472–479. doi:10.1299/jsmeb.41.472

Tuček, K., Carlsson, J., and Wider, H. (2006). Comparison of sodium and lead-cooled fast reactors regarding reactor physics aspects, severe safety and economical issues. *Nucl. Eng. Des.* 236, 1589–1598. doi:10.1016/j.nucengdes.2006.04.019

Wallis, G. B. (1974). The terminal speed of single drops or bubbles in an infinite medium. *Int. J. Multiph. Flow* 1, 491–511. doi:10.1016/0301-9322(74)90003-2

Wang, C., and Cai, J. (2018). Numerical simulation of bubble rising behavior in liquid LBE using diffuse interface method. *Nucl. Eng. Des.* 340, 219–228. doi:10.1016/j.nucengdes.2018.09.041

Zhang, C., Zhou, D., Sa, R., and Wu, Q. (2018). Investigation of single bubble rising velocity in LBE by transparent liquids similarity experiments. *Prog. Nucl. Energy* 108, 204–213. doi:10.1016/j.pnucene.2018.05.011

Zhang, Y., Liu, P., Xu, Y., and Tang, C. (2012). Three-dimensional volume of fluid simulations on bubble formation and dynamics in bubble columns. *Chem. Eng. Sci.* 73, 55–78. doi:10.1016/j.ces.2012.01.012